

Supplementary information

Glutathione-depleting reinforced enzyme catalytic  
activity for photothermal assisted bacterial killing by  
hollow mesoporous CuO

Hanzhu Shi,<sup>‡a</sup> Chengyang Ban,<sup>‡b</sup> Chenwei Dai,<sup>a</sup> Chengwang Li,<sup>a</sup> Xiuhong Zhou,<sup>a</sup> Ru  
Xia,<sup>b</sup> Jiasheng Qian<sup>b</sup> and Ming Cao<sup>\*b</sup>

<sup>a</sup>Anhui Academy of Medical sciences, Hefei, 230061, PR China

<sup>b</sup>Key Laboratory of Environment-Friendly Polymeric Materials of Anhui Province,  
School of Chemistry and Chemical Engineering, Anhui University, Hefei 230601, P. R.  
China

\*Corresponding author. Tel./fax: +86 551 63861163.

E-mail address: mcao@ahu.edu.cn

**Contents**

1. Chemicals
2. Characterization
3. Calculation of the photothermal conversion efficiency
4. Calculation of the Michaelis-Menten constant ( $K_m$ ) and maximum velocity ( $V_{max}$ )
5. **Fig. S1** SEM images of HM-CuO nanozymes formed by different mole ratio of  $Cu^{2+}$  and  $COO^-$  in the reaction system.
6. **Fig. S2** The O 1s spectra of the HM-CuO nanozymes.
7. **Fig. S3** The Michaelis-Menten fitting curves of ROS generation velocities versus  $H_2O_2$  concentration and the Lineweaver-Burke fitting (double reciprocal) of Michaelis-Menten fitting curve.
8. **Fig. S4** The catalytic effect of HM-CuO nanozymes at different pH value by using the TMB probe.
9. **Fig. S5** The catalytic effect of HM-CuO nanozymes under different conditions at different time with/without NIR irradiation by using the TMB and OPDA probe.

10. **Fig. S6** GSH depletion by HM-CuO nanozymes with different concentrations of HM-CuO nanozymes and GSH at different reaction times.

11. **Fig. S7** GSH-depleting percent by different concentrations of HM-CuO nanozymes.

### Chemicals

Polyacrylic acid sodium salt (PAAS, Mw = 2100) was purchased from Sigma-Aldrich Chemical Reagent Co., Ltd. Isopropyl alcohol (IPA) was obtained from Macklin Chemical Reagent Co., Ltd. Copper chloride dihydrate ( $\text{CuCl}_2 \cdot 2\text{H}_2\text{O}$ ) and hydrogen peroxide ( $\text{H}_2\text{O}_2$ , 30 wt%) were obtained from Sinopharm Chemical Reagent Co., Ltd. 3, 3', 5, 5'-Tetramethylbenzidine (TMB), O-phenylenediamine (OPDA), glutathione (GSH) and 5, 5'-dithio-bis (2-nitrobenzoic acid) (DTNB) were bought from Aladdin Chemical Reagent Co., Ltd. Deionized (DI) water was used in all experiments. All reagents were purchased from commercial sources and used without any further purification.

*Escherichia coli* (*E. coli*) and *Staphylococcus aureus* (*S. aureus*) are representative of Gram positive and Gram negative bacteria, and the separation rate of these two bacteria is the best among the positive and negative bacteria, respectively. *E. coli* (DH5 $\alpha$ ) and *S. aureus* (ATCC6538) were obtained from the Bena Biotechnology Co., Ltd.

### Characterization

Scanning electron microscopy (SEM) images were obtained using an S-4800 field-emission scanning electron microscope (Hitachi, Japan). Transmission electron microscopy (TEM) was performed on a JEM-2100 transmission electron microscope (Hitachi, Japan). The phase structure and element existence state were determined by X-ray powder diffraction (XRD, Rigaku SmartLab 9kW advance), X-ray photoelectron spectrometer (XPS, ESCALab 250Xi). Fourier transform infrared (FTIR) spectra and Thermogravimetric (TG) analyses were obtained on a Thermo Fisher TG-209F3 analyzer, and TG analyses were conducted by heating the samples from 25 to 800 °C at the rate of 10 °C/min. The  $\text{N}_2$  adsorption-desorption isotherms and corresponding pore size distribution were obtained on a Micromeritics ASAP 2460 instrument. UV-vis absorption spectroscopy was performed on Lambda 365 spectrophotometer (Perkin Elmer, USA). The photothermal data and thermal imaging pictures were recorded by using an IR thermal camera (T 1040, FLIR).

### Calculation of the photothermal conversion efficiency

The HM-CuO nanozymes photothermal conversion efficiency was calculated according to the previous literature.

$$\eta = \frac{hS(T_{\max} - T_{\text{surr}}) - Q_{\text{dis}}}{I(1 - 10^{-A_{808}})} \quad (1)$$

$\eta$  is the HM-CuO nanozymes photothermal conversion efficiency,  $T_{\max}$  are the equilibrium temperature for solution,  $T_{\text{surr}}$  is the surrounding temperature.  $Q_{\text{dis}}$  is the

heat loss.  $I$  is the incident laser power, and  $A$  is the absorbance of HM-CuO nanozymes at 808 nm.

$$\tau_s = \frac{m_i c_i}{hS} \quad (2)$$

$m_i$  is the mass of solvent and  $c_i$  is the heat capacity.  $\tau_s$  is the sample system time constant.

In brief,  $\tau_s$  is equal to 230.75 s,  $m$  is 0.63 g and  $C$  is  $4.2 \times 10^3 \text{ J}/(\text{kg} \cdot ^\circ\text{C})$ ,  $hS$  can be calculated to be  $0.01147 \text{ W}/^\circ\text{C}$ . Substituting  $I = 1.2 \text{ W}/\text{cm}^2$ ,  $A_{808} = 0.3128$ ,  $T_{\text{max}} - T_{\text{surr}} = 18.7 \text{ }^\circ\text{C}$  into Eq. (1), the photothermal conversion efficiency of HM-CuO nanozymes can be determined to be 34.82 %.

#### Calculation of the Michaelis-Menten constant ( $K_m$ ) and maximum velocity ( $V_{\text{max}}$ )

Based on TMB results, we calculated the  $K_m$  and  $V_{\text{max}}$ , all average initial velocities of absorbance changes would then be converted as initial velocities ( $V_0$ ) of ROS formation via the Beer Lambert law (Eq. 1), which were then plotted against the corresponding concentration and fitted with Michaelis Menten curves (Figure S5A). To determine the  $K_m$  and  $V_{\text{max}}$ , a linear double-reciprocal plot (Eq. 2) was obtained as given in Figure S5B. According to the calculation, the  $K_m$  and  $V_{\text{max}}$  values were calculated to be 0.0608 mM and  $0.4605 \times 10^{-8} \text{ mM s}^{-1}$  for HM-CuO nanozymes.

$$V_0 = \frac{A}{\epsilon b \Delta t} \quad (1)$$

$$\frac{1}{V} = \left(\frac{K_m}{V_{\text{max}}}\right)\left(\frac{1}{S}\right) + \left(\frac{1}{V_{\text{max}}}\right) \quad (2)$$

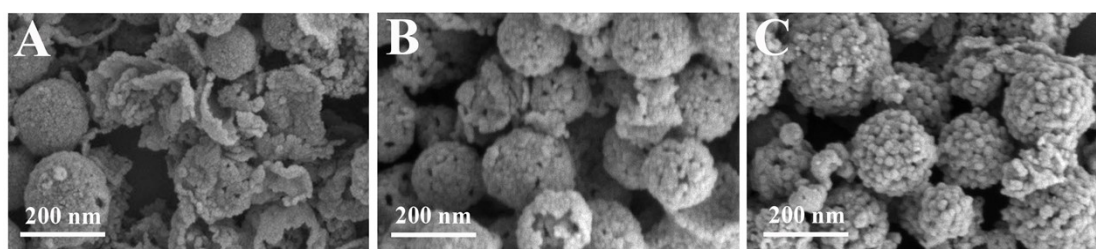


**Fig. S1** SEM images of HM-CuO nanozymes formed by mole different ratio of  $\text{Cu}^{2+}$  and  $\text{COO}^-$  in the reaction system: (A) 1:4, (B) 1:2, (C) 1:1.

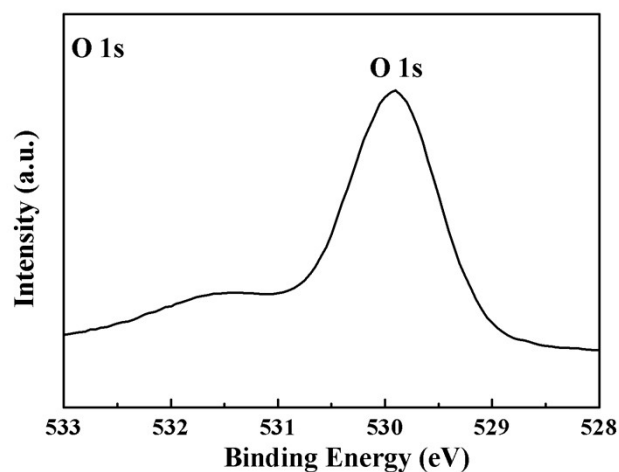


**Fig. S2** The O 1s spectra of the HM-CuO nanozymes.

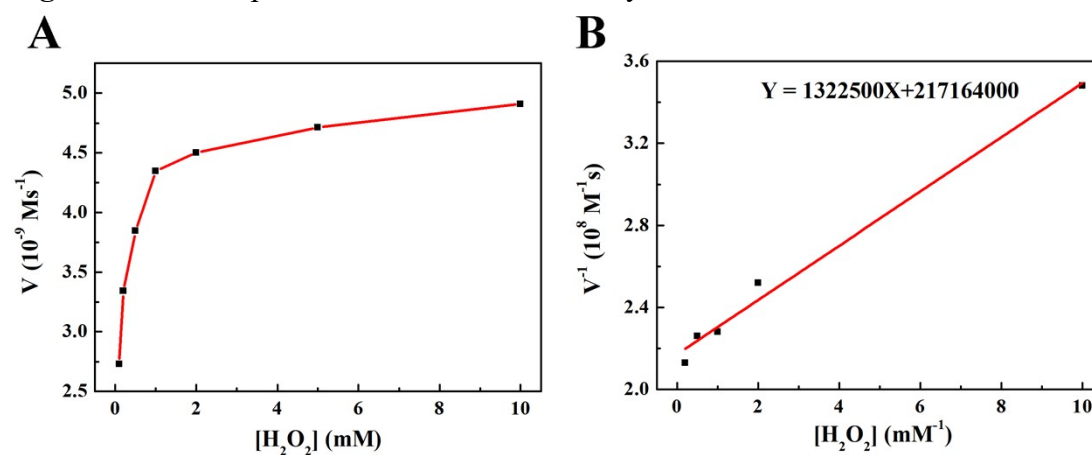


**Fig. S3** (A) The Michaelis-Menten fitting curves of ROS generation velocities versus  $\text{H}_2\text{O}_2$  concentration; (B) the Lineweaver-Burke fitting (double reciprocal) of Michaelis-Menten fitting curve.

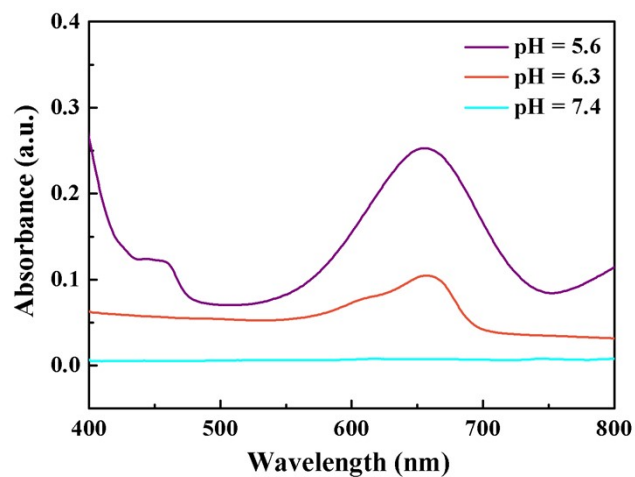


**Fig. S4** The catalytic effect of HM-CuO nanozymes at different pH value by using the TMB probe.

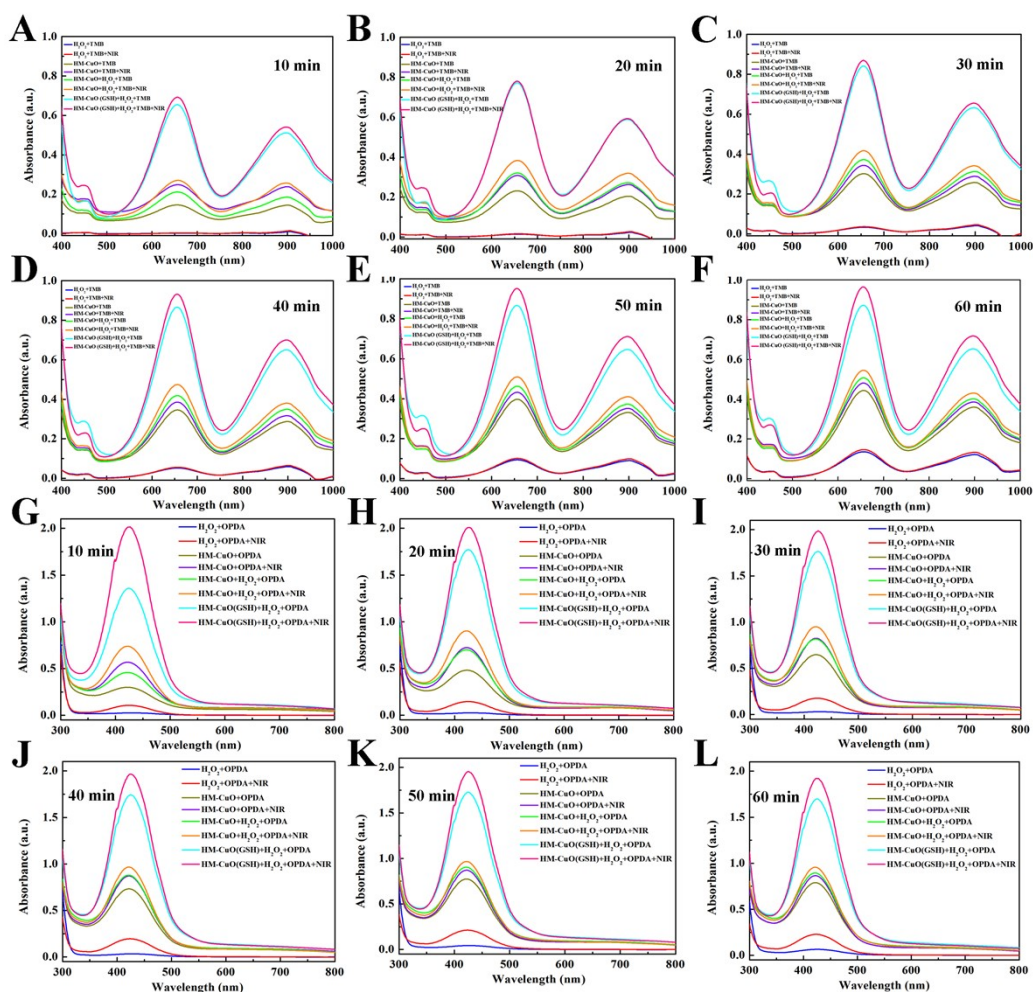


**Fig. S5** (A-F) The catalytic effect of HM-CuO nanozymes under different conditions at different time with/without NIR irradiation ( $1.2 \text{ W/cm}^2$ , 10 min) by using the TMB probe. (G-L) The catalytic performance of HM-CuO nanozymes under different conditions at different time with/without NIR irradiation ( $1.2 \text{ W/cm}^2$ , 10 min) by using the OPDA probe.

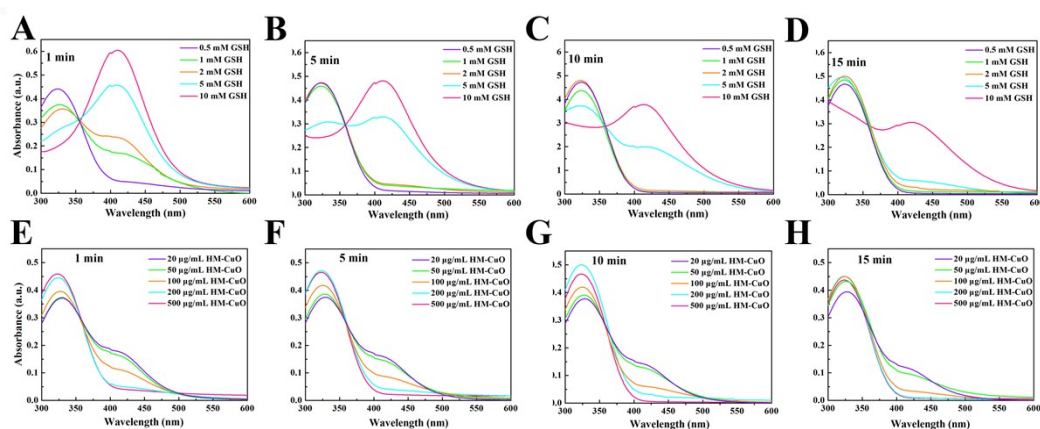


**Fig. S6** (A-D) GSH depletion by HM-CuO nanozymes with different GSH concentrations (0.5, 1.0, 2.0, 5.0, 10.0 mM) at different reaction times (1, 5, 10, 15 min).

(E-H) GSH depletion by HM-CuO nanozymes of different concentrations (20, 50, 100, 200, 500  $\mu\text{g/mL}$ ) at different reaction times (1, 5, 10, 15 min).

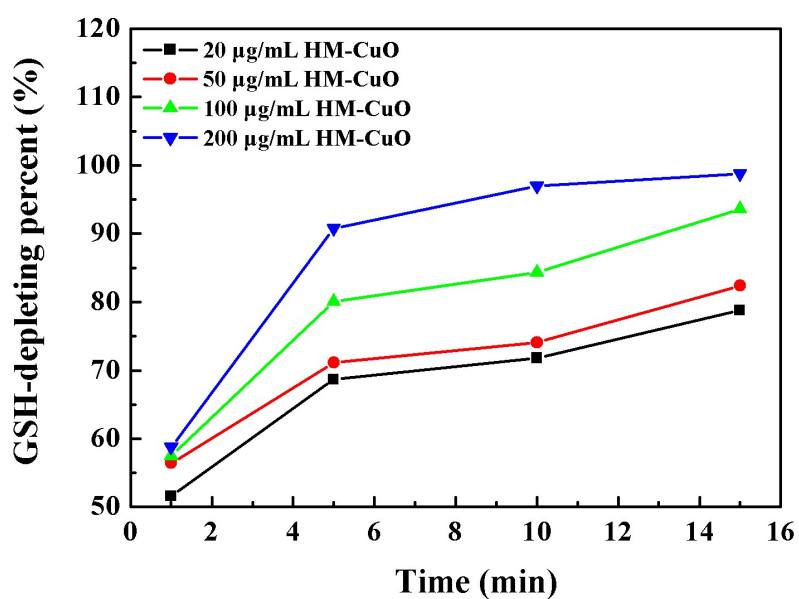


**Fig. S7** GSH-depleting percent by different concentrations of HM-CuO nanozymes (20, 50, 100, 200, 500  $\mu\text{g/mL}$ ).